$\pi\pi \rightarrow \pi\pi$ cross sections near threshold

M. Kermani,[1] O. Patarakin,[2] G. R. Smith,[5,*] P. A. Amaudruz,[5] F. Bonutti,[3,4] J. T. Brack,[5,†] P. Camerini,[3,4] L. Felawka,[5] E. Fragiacomo,[3,4] E. F. Gibson,[6] N. Grion,[3] G. J. Hofman,[1,†] E. L. Mathie,[7] S. McFarland,[1] R. Meier,[5,‡] D. Ottewell,[5] K. J. Raywood,[1] R. Rui,[3,4] M. E. Sevior,[8] R. Tacik,[7] V. Mayorov,[2] and V. Tikhonov[2]

(The CHAOS Collaboration)

[1]*Physics Department, University of British Columbia, Vancouver, British Columbia, Canada V6T 2A6*

[2]*General and Nuclear Physics Institute, RRC Kurchatov Institute, Moscow 123182, Russia*

[3]*Istituto Nazionale di Fisica Nucleare, 34127 Trieste, Italy*

[4]*Dipartimento di Fisica dell'Universita' di Trieste, 34127 Trieste, Italy*

[5]*TRIUMF, Vancouver, British Columbia, Canada V6T 2A3*

[6]*California State University, Sacramento, California 95819*

[7]*University of Regina, Regina, Saskatchewan, Canada S4S 0A2*

[8]*School of Physics, University of Melbourne, Parkville, Victoria, 3052, Australia*

(Received 3 June 1998)

An analysis of new data for the reaction $\pi^{\pm}p \rightarrow \pi^{\pm}\pi^{+}n$ at incident energies between 223 and 284 MeV is presented. $\pi^{+}\pi^{-}$ cross sections are obtained via Goebel-Chew-Low techniques by extrapolation to the pion pole using the pseudoperipheral approximation. A consistency check between the present experimental results and previous experiments at higher energies is made using Roy equations. The isospin 0, *S*-wave $\pi\pi$ scattering length was obtained using a variety of methods. The result obtained from a threshold expansion is $a_0^0 = 0.204 \pm 0.014$ (statistical) ± 0.008 (systematic) in inverse pion mass units. It is shown that there are significant differences between the reaction mechanisms for the $(\pi^{-}\pi^{+})$ and $(\pi^{+}\pi^{+})$ channels. [S0556-2813(98)00212-X]

PACS number(s): 13.75.Lb, 13.60.Hb, 13.60.Le, 13.75.Gx

I. INTRODUCTION

The application of QCD in the low-energy regime through the use of effective Lagrangians such as employed in chiral perturbation theory [1,2] has made low-energy $\pi\pi$ scattering of great interest. $\pi\pi$ scattering observables provide a sensitive tool for studying the explicit breaking of chiral symmetry in strong interactions. Interest has focused on the region near threshold since in the chiral limit, the $\pi\pi$ scattering lengths vanish there exactly. A measure of these threshold parameters is therefore an explicit measure of chiral symmetry breaking. Moreover, $\pi\pi$ scattering observables are required to establish other parameters of chiral perturbation theory and other effective low-energy models. Currently our progress understanding these challenging problems is hindered by the absence of accurate $\pi\pi$ scattering cross sections near threshold.

$\pi\pi$ scattering lengths and phase shifts have been deduced [3] from $\pi N \rightarrow \pi\pi N$ reactions in the GeV regime using Goebel-Chew-Low analysis [4]. In this case the required information is obtained by isolating the contribution of the one-pion exchange (OPE) diagram via extrapolation to the pion pole. In the past, this approach has been used for incident pion momenta p_{π} in the 4–10 GeV/c range, and a review of these works is presented in Refs. [5–7]. The extrapolation procedure is not strictly unambiguous since the contribution of the non-OPE components (Δ, N^*) can affect the reliability of the results. However, the near threshold region $(m_{\pi\pi}^2 \gtrsim 4)$ is most sensitive to the scattering lengths, and the determination of $\pi\pi$ cross sections in this region would represent an important step towards understanding $\pi\pi$ interactions. The only Goebel-Chew-Low analysis of $\pi N \rightarrow \pi\pi N$ reactions in the near threshold region was a very limited statistics photoemulsion experiment [8] which obtained the result $a_0^0 = 0.24 \pm 0.09$.

In the present paper we make an attempt to determine $\pi\pi$ scattering parameters in the region of prime importance: in the vicinity of threshold. The data on the $\pi^{-}p \rightarrow \pi^{+}\pi^{-}n$ and $\pi^{+}p \rightarrow \pi^{+}\pi^{+}n$ interactions required to this end were obtained for projectile kinetic energies $223 \leqslant T_{\pi} \leqslant 285$ MeV with the CHAOS spectrometer [9] at TRIUMF. Details of the experiment, as well as the results of model calculations applied to total and single differential cross sections, are presented in a companion article [10]. In the present work, we concentrate exclusively on the double differential cross sections, Goebel-Chew-Low analysis, and determination of the $\pi\pi$ scattering length $a_L^I = a_0^0$. In the following we make use of the variables $m_{\pi\pi}$ (the dipion invariant mass), t (the square of the four-momentum transfer to the nucleon), and θ (the angle between the two negative pions in the dipion rest frame). We express $m_{\pi\pi}^2$ and t in units of the pion mass squared $(\mu^2 = m_{\pi}^2)$.

Previous experiments are briefly summarized in Sec. II. We describe some of the experimental features most relevant to the present work in Sec. III. In Sec. IV we describe the Goebel-Chew-Low analysis, which utilizes the new CHAOS double differential cross section data and the pseudoperipheral prescription employed by Baton *et al.* [3].

*Corresponding author. Electronic address: smith@triumf.ca

†Present address: University of Colorado, Boulder, CO 80309.

‡Present address: Physikalisches Institut, Universität Tübingen, 72076 Tübingen, Germany.

In Sec. V the dispersion constraints embodied in Roy's equations are used to check whether or not the resulting near-threshold $\sigma_{\pi\pi}(m_{\pi\pi})$ determined from the new CHAOS data are consistent with results obtained from other experiments at much higher incident pion momenta. In Sec. VI we make use of the new CHAOS $\sigma_{\pi\pi}(m_{\pi\pi})$ data to determine the *S*-wave scattering length a_0^0 which can be compared directly to the most recent predictions [11–13] from chiral perturbation theory. A discussion and conclusions are presented in Sec. VII.

II. PREVIOUS EXPERIMENTS

Experimental evaluation of $\pi\pi$ scattering observables is difficult because only indirect methods are available. Several processes have been studied in the past or are proposed as a means to obtain $\pi\pi$ scattering parameters.

To date, the most reliable measure of the $\pi\pi$ scattering lengths comes from the study of K_{e4} decays. An analysis of 30 000 decays yielded the result $a_0^0 = 0.28 \pm 0.05 \mu^{-1}$ [14]. In this method, both final state pions are on the mass shell and are the only strongly interacting particles in the final state, however, the branching ratio is only $\sim 4 \times 10^{-5}$. New results with much better statistics are expected from both BNL and DAΦNE.

The $e^+e^- \rightarrow \pi^+\pi^-$ reaction proceeds through one-photon annihilation and provides information on the odd $\pi\pi$ scattering partial waves. For example, in Ref. [15] the *P*-wave scattering length $a_1^1 = 0.036 \pm 0.010$ was obtained from an analysis of the pion form factors.

$\pi^+\pi^-$ atoms have the potential to provide a measure of $|a_0^0 - a_0^2|$ at the 5% level. An elegant experiment has been proposed at CERN [16]. A search at IUCF [17] failed to detect a signature of pionium.

So far only K_{e4} decays and $\pi N \rightarrow \pi\pi N$ reactions have proven useful in studying $\pi\pi$ scattering near threshold, and only $\pi N \rightarrow \pi\pi N$ reactions can give any information about $\pi\pi$ scattering parameters as a function of energy. The most relevant $\pi N \rightarrow \pi\pi N$ experiments and their results for the scattering lengths are as follows.

In 1974 a low statistics bubble chamber experiment explored the $(\pi^+\pi^-)$ and $(\pi^-\pi^0)$ channels at an incident pion momentum of 415 MeV/c [18]. Using an isobar model along with data acquired at higher energies, they found $-0.06\mu^{-1} < a_0^0 \leq 0.03\mu^{-1}$, which is consistent with zero.

The OMICRON group at CERN measured total cross sections and angular distributions for the $(\pi^+\pi^-)$, $(\pi^-\pi^0)$, and $(\pi^+\pi^+)$ channels at incident pion momenta between 295 and 450 MeV/c [19–21]. The OMICRON data were analyzed in the context of the Olsson and Turner (OT) model [22]. This model assumes that OPE is the dominant mechanism close to threshold, and it parameterizes the threshold $(\pi,2\pi)$ amplitude and the $\pi\pi$ scattering lengths in terms of the chiral symmetry breaking parameter ξ. The OMICRON results for ξ and the scattering lengths (in units of inverse pion mass) are $\xi = -0.5 \pm 0.8$, $a_0^2 = -0.05 \pm 0.02$, $a_0^0 = 0.15 \pm 0.03$ for the $(\pi^+\pi^0)$ channel, $\xi = 0.1^{+0.5}_{-0.7}$, $a_0^2 = -0.03 \pm 0.02$, $a_0^0 = 0.18 \pm 0.04$ in the $(\pi^+\pi^-)$ channel, and $\xi = 1.56 \pm 0.26$, $a_0^2 = -0.08 \pm 0.01$ for the $(\pi^+\pi^+)$ channel.

A result very near the $\pi N \rightarrow \pi\pi N$ threshold was obtained recently [23], also within the context of the OT model. That experiment stopped a π^+ beam in a scintillator stack, and detected the final state neutron in coincidence with the pions. The $\pi\pi$ scattering length was determined to be $a_0^2 = -0.040 \pm 0.001 \pm 0.003$, with $\xi = -0.2 \pm 0.15$. A similar experiment [24] employing incident $\pi^\pm$ was analyzed in the context of heavy baryon chiral perturbation theory, and obtained the results $a_0^0 = 0.23 \pm 0.08$ and $a_0^2 = -0.031 \pm 0.008$. To date, these represent the experimental data acquired closest to the pion production threshold energy of 172.38 MeV.

Measurements of the $(\pi^0\pi^0)$ channel at pion incident energies ranging from 5 MeV above threshold to $T_\pi = 293$ MeV were performed at Brookhaven [25]. The total cross section data were interpreted in the context of the OT model. The value of ξ from this experiment is -0.98 ± 0.52. The corresponding *S*-wave $\pi\pi$ scattering lengths are $a_0^0 = 0.207 \pm 0.028$ and $a_0^2 = -0.022 \pm 0.011$.

In 1993, the Virginia group measured total cross sections as well as angular distributions at LAMPF for the $(\pi^+\pi^0)$ channel at incident pion energies of 190, 200, 220, 240, and 260 MeV [26,27]. They performed an analysis in which all of the existing $\pi N \rightarrow \pi\pi N$ were fitted to extract partial amplitudes in the framework of the OT model. Their results indicate that $\xi = -0.25 \pm 0.10$ and $a_0^2 = -0.041 \pm 0.001$.

III. DATA REDUCTION

The $\pi^\pm p \rightarrow \pi^+\pi^\pm n$ cross sections reported in this work were measured using a liquid hydrogen target and the CHAOS magnetic spectrometer [9] at TRIUMF. CHAOS is a ~ 1 sr detector composed of four cylindrical, concentric wire chambers which are surrounded by an array of scintillation and lead-glass Cerenkov counters.

Pion bombarding energies of 223, 243, 264, and 284 MeV were studied. The momentum width of the incident $\pi^+(\pi^-)$ beam was $\Delta p/p \sim 1\%(5\%)$. Typically 10 000 $\pi^+\pi^-$ and $\pi^+\pi^+$ events were recorded at each energy. All events were binned into a $10 \times 10 \times 10$ lattice of $m^2_{\pi\pi}$, t, and $\cos(\theta)$. A weighting factor determined from Monte Carlo simulation of the detector was applied on an event-by-event basis to account for the detector acceptance. Phase space was used to describe the out-of-plane behavior of the reaction. Previous experiments have shown [28,29] that for our incident pion energies, the out-of-plane deviations from phase space range from only $\sim 2\%$ at 223 MeV to $\sim 13\%$ at 284 MeV. Further arguments supporting the out-of-plane assumptions made in this work are put forward in Refs. [10,30]. The double differential cross sections $d^2\sigma/dm^2_{\pi\pi}dt$ obtained by integrating over $\cos(\theta)$ were used as input to the Goebel-Chew-Low analysis. The overall normalization was checked by measuring $\pi^- p$ elastic differential cross sections at each bombarding energy. We estimate that the systematic uncertainty associated with $d^2\sigma/dm^2_{\pi\pi}dt$ is $\sim 10\%$. Further details of the experimental procedure and data analysis are presented in Refs. [10,30].

IV. GOEBEL-CHEW-LOW ANALYSIS

The extraction of $\pi\pi$ scattering observables from $\pi N \rightarrow \pi\pi N$ data is usually based on isolating the contribution of

the one pion exchange (OPE) mechanism from background processes which involve resonance and isobar exchanges. This approach is referred to as Chew-Low analysis (properly, Goebel-Chew-Low analysis).

The basic idea behind the Goebel-Chew-Low procedure is as follows. The t dependence of the cross section for $\pi^- p \to \pi^+ \pi^- n$ has the form [5]

$$\frac{d\sigma}{dt} \sim \frac{t}{(t-1)^2} + X, \tag{1}$$

where the first term represents the OPE mechanism and X stands for all other processes (background). The t dependence of the numerator is of crucial importance since it indicates that the OPE contribution vanishes at $t=0$ (see, for example, Fig. 3.2.1 from Ref. [5]). In other words, the OPE process is peripheral. According to Eq. (1), as $t\to\mu^2$ (the pion pole) the first term diverges, and if the second term X remains finite, it is possible to isolate the OPE contribution from the rest. This implies that by extrapolating to $t=\mu^2=1$ one can remove off-shell effects and non-OPE contributions.

The Goebel-Chew-Low extrapolation function $F(t,m_{\pi\pi})$ is defined as

$$F(t,m_{\pi\pi}) = \frac{\pi p_\pi^2}{f^2} \frac{(t-1)^2}{m_{\pi\pi} q} \frac{d^2\sigma}{dt \cdot dm_{\pi\pi}^2}, \tag{2}$$

where $q=\sqrt{m_{\pi\pi}^2/4-1}$, and $f^2=0.08$ is the πN coupling constant. The pion exchanged in the OPE diagram is off-shell in the physical region. In the present paper we apply the pseudoperipheral approximation method (see, for example, Ref. [3]), in which an auxiliary function $F'=F/|t|$ is extrapolated to the pion pole ($t=\mu^2$). This method makes use of the fact that in the case of OPE dominance, $F'(t,m_{\pi\pi})$ is linear in t, which implies $F(0,m_{\pi\pi})=0$. The on-shell $\pi^+\pi^-$ scattering cross section, $\sigma_{\pi\pi}(m_{\pi\pi})$ is equal to $F'(t=+1,m_{\pi\pi})$.

A. OPE dominance

Although the Goebel-Chew-Low procedure assumes OPE dominance in the region where t is near the physical threshold, it follows from the pseudo-scalar nature of the pion that the OPE contribution vanishes at $t=0$ [5]. In addition, the OPE signal diminishes for $t\ll 0$. The t dependence of the first term in Eq. (1) is shown in Fig. 1, normalized to its maximum in the physical region. From this figure, it is clear that in the physical region ($t<0$), $\sigma_{\rm OPE}$ has a maximum at $t=-1$ and that the region where $\sigma_{\rm OPE}$ is at least half this maximum is $-6<t<-0.2$. In order to maximize the contribution of OPE relative to the background, therefore, it would seem prudent to stay inside the approximate range $-6<t<-0.2$. It should, however, be noted that the maximum kinematically allowed value of t is less than zero. For the energies covered in this experiment, $t_{\rm max}$ varies from -0.6 to -0.3.

Beyond this guidance, there are two additional tests for OPE dominance, which unfortunately do not qualify as proofs. First, the OPE contribution should be S wave. Second, F' must be linear in the t interval over which the extrapolation is performed. If linearity is not observed in the interval where OPE is expected to dominate, then the extrapolation cannot be performed because the assumption of OPE dominance cannot be supported. On the other hand, if nonlinearities in F' are observed outside the region where OPE is expected to dominate, this does not prevent the application of the Goebel-Chew-Low procedure in the linear region. In fact, nonlinear regions are expected to appear somewhere, since it is generally known that background (Δ and N^*) processes can contribute significantly to $\pi^- p \to \pi^+ \pi^- n$. The question is only in which $m_{\pi\pi}^2$ bins, for which incident energies, and over which t intervals this background dominates sufficiently to destroy the linearity expected for the OPE mechanism.

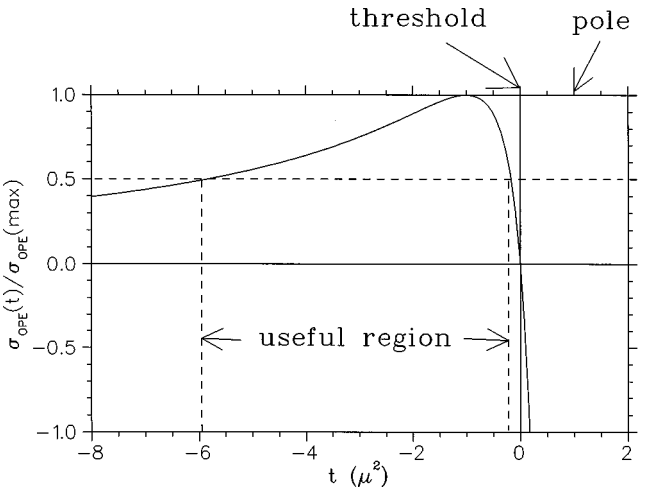

FIG. 1. The first term of Eq. (1), which represents the OPE contribution to the cross section, is divided by its maximum and plotted as a function of t. The physical regions where OPE reaches 50% of its maximum ($t=-1$) value are indicated along with the physical region ($t<0$), threshold ($t=0$), and pion pole ($t=+1$).

B. Data selection

A careful selection of the data used in the Goebel-Chew-Low analysis was necessary for three reasons. First, as discussed above, the hypothesis of OPE dominance requires that the extrapolation function F' be linear in t, so nonlinear regions in t should be excluded from the analysis. Second, the Goebel-Chew-Low extrapolation should yield a physically meaningful result. In other words, a positive value for $F'(t=1)$. Presumably, both of these rejection criteria can arise when the data in question fall outside the region of OPE dominance. Third, kinematic limits have the effect of rendering some of the $F'(t)$ bins at the edges of the observed distributions empty or only partially filled. These bins should be excluded from the fits, obviously.

Although it is easy to devise safe and rigorous tests for the latter two rejection criteria, the first requirement of linearity is more subjective and can potentially lead to bias in the data selection. Therefore, two methods for data selection were pursued.

For the first method (A) our philosophy was to use data rejection sparingly and only in clear-cut cases. A set of rules was devised which was applied separately to each $m_{\pi\pi}^2$ bin.

(1) If the extrapolated $F'(T_\pi, t=1, m^2_{\pi\pi})<0$, then the data for that energy and $m^2_{\pi\pi}$ bin were rejected. (2) If F' was zero anywhere in the interval $-6<t<-2$ then the data for that energy and $m^2_{\pi\pi}$ bin were rejected. (3) Otherwise, the data in the interval $-6<t<-2$ were always kept. (4) The $t>-1.0$ data were always excluded. (5) Data at the edges of each distribution ($t=-1.1,-1.9$ and $t=-6.5,-7.5$) were rejected if and only if either (a) the bin was empty or (b) the point was more than five standard deviations from the line determined without it (i.e., partially empty).

The rationale for these rules and their impact is as follows. The first rule simply rejected unphysical results. The $\pi\pi$ cross section has to be positive. If the extrapolation delivered a negative result then it was assumed that background mechanisms spoiled the extrapolation. All the 300 MeV data, as well as the 280 MeV $m^2_{\pi\pi}=4.15$ data were rejected this way. The second rule was enforced because in the interval $-6<t<-2$, OPE should dominate. If F' is small in this interval then OPE dominance cannot safely be assumed. This eliminated the sparse data at 220 MeV for all bins with $m^2_{\pi\pi}>4.15$, and the 240 MeV data at the largest $m^2_{\pi\pi}$ bin, $m^2_{\pi\pi}=5.65$.

Rule three was enforced to avoid introducing bias into the data selection. We experimented with data rejection in this interval in method B (discussed below), and obtained much better fits as a result. For method A we wanted to pay the χ^2 penalty, keep all the points in the primary interval $-6<t<-2$, and compare the results to those obtained with the more restrictive data selection method B.

The fourth rule accounted for the fact that the first two bins at $t=-0.3$ and -0.6 were almost always empty, and in the few cases where they were not empty it was likely that they were only partially filled. The kinematic limits, coupled with the steep t dependence of the OPE mechanism in this region (see Fig. 1), made use of data in this interval questionable. Finally, the last rule also tried to account for empty and partially empty bins at the edges of our distributions which reflected the kinematic limits available. At a given incident pion energy and dipion invariant mass, the kinematically allowed region in t is limited. It is possible that the diminishing contribution of OPE as $|t|$ increases may also be responsible for some of the nonlinearity occasionally observed at large $|t|$. Empty bins were discarded for all $m^2_{\pi\pi}$ bins at $t=-7.5$, 240 MeV as well as $t=-6.5$, $m^2_{\pi\pi}=4.15$, 220 MeV. The 5σ test eliminated a few points at the edges of the three highest $m^2_{\pi\pi}$ bins for 240 and 260 MeV.

Data selection method B took the opposite philosophy of method A, and attempted to identify and reject statistical outliers which affected the quality of the fits but not the extrapolated $\sigma_{\pi\pi}$. Method B started with the data which were selected by method A. Each global Goebel-Chew-Low fit was examined to find the point with the largest individual χ^2 contribution greater than 5. This point was then dropped and the Goebel-Chew-Low fit repeated to check whether or not the resulting $\sigma_{\pi\pi}(m^2_{\pi\pi})$ moved by more than one standard deviation or not. If it did (only at $m^2_{\pi\pi}=4.45$) then the point was kept, otherwise it was rejected. The procedure was repeated until no more points with an individual χ^2 greater than 5 were found, checking each time that the extrapolated $\sigma_{\pi\pi}(m^2_{\pi\pi})$ did not move more than 1σ. As a result, several points were rejected by method B in each $m^2_{\pi\pi}$ bin which had been accepted by method A.

TABLE I. Table of points dropped in the data selection process B, and the corresponding effect on the cross section and χ^2 of the fit. Entries tagged gbl and A indicate the starting values associated with the global fit using data selection method A. The next to last column indicates the total χ^2. N_{data} refers to the number of data points used in each global fit.

$m^2_{\pi\pi}$	T_π (MeV)	t	σ (mb)	χ^2	N_{data}
4.15	gbl	A	4.38±0.61	45	21
	264	-2.63	5.08±0.65	32	20
	223	-3.50	4.35±0.69	24	19
4.45	gbl	A	4.89±0.45	96	23
	264	-1.88	5.40±0.48	78	22
	243	-5.50	4.87±0.49	56	21
4.75	gbl	A	6.42±0.58	100	23
	284	-7.50	6.21±0.59	55	22
	264	-1.88	5.92±0.60	45	21
	243	-2.63	5.96±0.60	35	20
	243	-1.88	6.26±0.61	29	19
5.05	gbl	A	7.26±0.77	44	22
	264	-1.13	6.67±0.79	28	21
	243	-1.88	7.85±0.87	18	20
5.35	gbl	A	9.21±2.03	38	17
	264	-4.50	8.03±2.07	27	16
	243	-5.50	7.30±2.09	20	15
5.65	gbl	A	4.85±1.99	30	11
	284	-6.50	5.41±2.07	22	10
	284	-7.50	5.70±2.65	14	9
	264	-5.50	5.84±3.15	9	8

The points rejected by method B are listed in Table I. The overall χ^2 of the Goebel-Chew-Low fits using data selection method B were markedly better than method A, however, the results of the extrapolations were the same to within 1σ for both methods.

C. Analysis of the $\pi^- p \to \pi^+ \pi^- n$ reaction

The Goebel-Chew-Low extrapolations must be performed under conditions which enhance the OPE contribution and suppress the background. In the present work this was accomplished by carefully choosing the t intervals over which the Goebel-Chew-Low fits were made. Suitable t intervals were selected such that $F'(t, m_{\pi\pi})$ could be described by a linear function. The parameters of the linear fit were used to determine the on-shell $\pi^+\pi^-$ scattering cross section by extrapolation to the pion pole. The central values of the t bins in units of inverse pion mass squared were -0.250, -0.625, -1.125, -1.875, -2.625, -3.500, -4.500, -5.500, -6.500, and -7.500.

The OPE contribution should be S wave [31]. A partial wave decomposition [10] of the $\cos\theta$ angular distributions measured in the $\pi^- p \to \pi^+ \pi^- n$ channel indicate a P-wave scattering amplitude between 5 and 10 % of the S-wave amplitude, depending on the incident pion energy. This further emphasizes the importance of a careful data selection for the Goebel-Chew-Low extrapolations, since some P wave is present in the data. The worst case is at 305 MeV (10% P

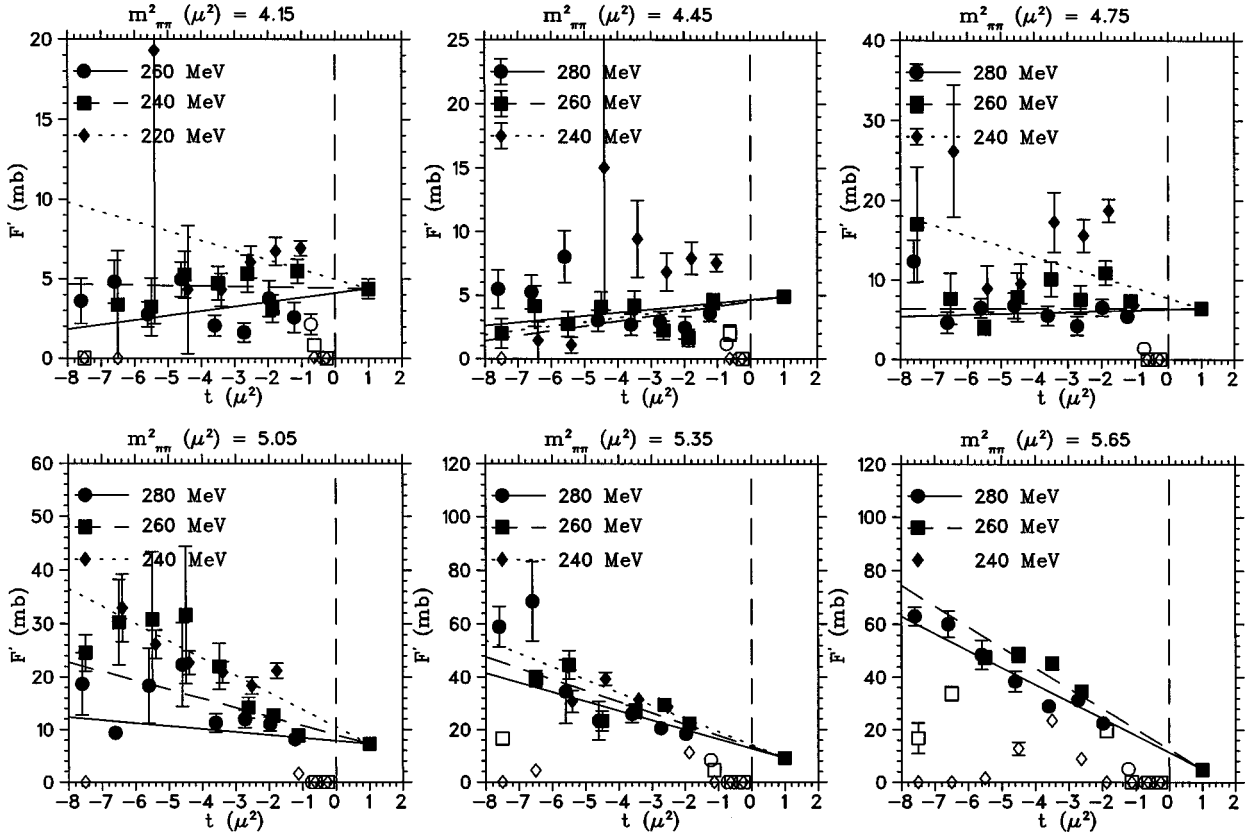

FIG. 2. The values of $F'(T_\pi,t,m^2_{\pi\pi})$ are plotted as a function of t for each of the incident energies and $m^2_{\pi\pi}$ bins used in the Goebel-Chew-Low analysis. Solid points indicate those chosen by the data selection method A, open points were dropped. The global Goebel-Chew-Low fits according to Eq. (3) are also plotted as straight lines. The points at $t=+1$ shown for each $m^2_{\pi\pi}$ bin were not measured, they indicate the value of the extrapolation and correspond to $\sigma_{\pi\pi}(m^2_{\pi\pi})$.

wave). That energy was eliminated from the analysis.

Those regions where the background is competitive with OPE have to be avoided. Since there is no way to guarantee these regions have been successfully avoided in our analysis, however, it is impossible to be certain that the cross sections derived here correspond to OPE, or that the scattering length we obtain is reliable in this context. This clearly weakens the impact of our results, and underscores the importance of obtaining more precise K_{e4} results for the scattering length.

No attempt was made to remove potential background contributions in this work, since there exists no reliable model for such a procedure. Instead, we relied on the tests of OPE dominance discussed above, restricted our analysis to those regions where F' was linear in t, and otherwise followed the same Goebel-Chew-Low procedure as has been applied at higher energies [3] with one important difference: our experiment enjoys the advantage relative to previous Goebel-Chew-Low analyses that we have results at several energies.

We capitalized on this by using all the available data for each $m^2_{\pi\pi}$ bin (for all incident energies). In other words, a global fit was performed for each $m^2_{\pi\pi}$ bin which simultaneously made use of the data available at each energy. If the extrapolated value of $F'(T_\pi,t=+1,m^2_{\pi\pi})$ is $\sigma_{\pi\pi}(m^2_{\pi\pi})$, then in practice we must obtain the same result independently of the initial energy. In this case we can write

$$F'(T_\pi,t,m^2_{\pi\pi})=\sigma_{\pi\pi}(m^2_{\pi\pi})+\alpha(T_\pi,m^2_{\pi\pi})\times(t-1), \tag{3}$$

where $\sigma_{\pi\pi}(m^2_{\pi\pi})$ and $\alpha(m^2_{\pi\pi},T_\pi)$ are free parameters, and F' was derived from the individual measured double differential cross sections according to Eq. (2). The fits were performed using a multiple linear regression method [32] which accounted for the statistical uncertainties in the data. Typically, each bin of $m^2_{\pi\pi}$ for which the global fit was performed consisted of 7 or 8 values of $F'(t)$, at each of three energies, corresponding to a total of four free parameters [the $\sigma_{\pi\pi}(m^2_{\pi\pi})$, and a slope at each energy] determined from more than 20 data points.

The data, fits, and extrapolations are shown in Fig. 2. All the data used in the determination of $\sigma_{\pi\pi}$ and a_0^0 (discussed below) are included in these figures as solid points. Open points denote those which were dropped from the analysis according to the data selection criteria A discussed above. The extrapolated cross sections are listed in Table II. The errors shown in Table II reflect the uncertainty in the fitted parameter $\sigma_{\pi\pi}(m^2_{\pi\pi})$, which accounts for the statistical error of each data point, but not the systematic ($\sim$10%) uncertainty in the cross sections. The impact of the systematic error on the determination of a_0^0 is discussed in Sec. VI.

The overall χ^2_ν obtained from the global fits with method A for each bin was poor. We obtained $\chi^2_\nu=2.5$, 4.6, 5.0, 2.2, 2.7, and 3.4 for the dipion invariant mass bins $m^2_{\pi\pi}=$ 4.15, 4.45, 4.75, 5.05, 5.35, and 5.65, respectively. The lowest energy data in each $m^2_{\pi\pi}$ bin contribute the most to these χ^2_ν values, especially for the two worst cases at $m^2_{\pi\pi}=$ 4.45 and

TABLE II. Table of $\pi\pi$ results.

Obs.	Data	Method	$m^2_{\pi\pi}=4.15$	4.45	4.75	5.05	5.35	5.65	a_0^0	b_0^0
F' (mb)	A	1	4.38±0.61	4.89±0.45	6.42±0.58	7.26±0.77	9.21±2.03	4.85±1.99	0.204±0.014	0.420±0.118
χ^2_ν			2.5	4.8	5.0	2.3	2.7	3.3	1.2	
	A	2							0.229±0.008	0.184
χ^2_ν									2.1	
δ_0^0 (deg)	A	3	2.29±0.15	4.29±0.19	6.40±0.28	8.12±0.42	10.39±1.08	8.63±1.60	0.195±0.013	0.424±0.071
χ^2_ν									1.1	
F' (mb)	B	1	4.35±0.69	4.83±0.49	6.25±0.60	7.85±0.87	7.32±2.09	5.84±3.15	0.198±0.011	0.482±0.103
χ^2_ν			1.6	3.3	1.9	1.1	1.8	1.8	1.2	
	B	2							0.229±0.008	0.184
χ^2_ν									2.1	
δ_0^0 (deg)	B	3	2.28±0.16	4.27±0.19	6.32±0.29	8.42±0.40	9.33±1.21	9.38±1.47	0.193±0.013	0.435±0.071
χ^2_ν									1.0	
F' (mb)	C	4		3.2±0.5	8.0±0.7	6.8±0.8	7.5±5.4	5.7±3.6	0.209±0.011	

4.75. On the other hand, the two higher energies in each $m^2_{\pi\pi}$ bin are typically nearly colinear, have smaller uncertainties, and dominate the global fits.

The poor values of χ^2_ν obtained from the global Goebel-Chew-Low fits incorporating data selection method A were the motivating factor behind reanalysis of the data with method B. The χ^2_ν of the global fits with data selection method B were 1.6, 3.3, 1.9, 1.1, 1.8, and 1.8 for the same $m^2_{\pi\pi}$ bins listed above. Although in a couple of cases the slopes of the lines through the data differed considerably in methods A and B, the extrapolated $F'(t=+1,m^2_{\pi\pi})$ was the same to within much less than one standard deviation in both methods. This fact alleviated much of the initial concern we had with the poor χ^2_ν obtained with method A. At the same time it is reassuring to see that an almost complete data selection gives the same results as a much more restrictive one. The $\pi\pi$ cross sections derived from data selection B are also provided in Table II.

For the largest $m^2_{\pi\pi}$ bins ($m^2_{\pi\pi}>5.65$), linear regions in F' could not be found. A typical F' distribution for one of these large $m^2_{\pi\pi}$ bins is shown in Fig. 3. Although it is unfortunate that some of the available data could not be used in the Goebel-Chew-Low analysis, it is on the other hand comforting to see regions where background mechanisms apparently do dominate, since we know they contribute to the overall strength of the reaction. Fortunately, there seem to be other regions ($m^2_{\pi\pi}<5.65$) where they do not dominate. Even more fortunately, these regions are close to threshold where the sensitivity to the scattering length is greatest.

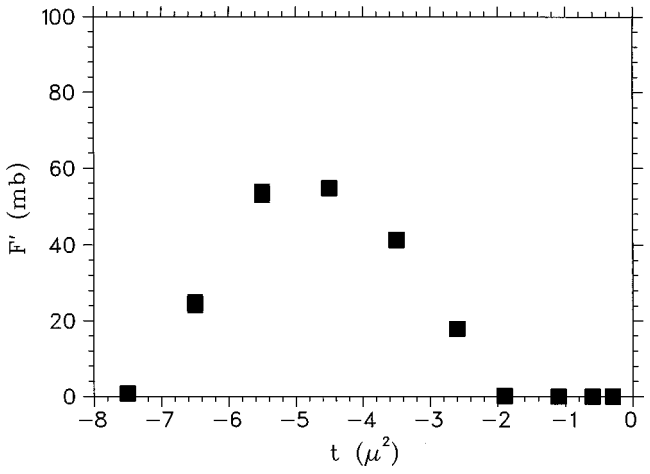

FIG. 3. The Goebel-Chew-Low extrapolation function F' at 284 MeV, $m^2_{\pi\pi}=6.55$, is shown to illustrate the nonlinearity observed for these higher dipion invariant mass bins.

D. Analysis of the $\pi^+p\to\pi^+\pi^+n$ reaction

In principle the same Goebel-Chew-Low technique may also be applied to the $(\pi^+\pi^+)$ data, and the results used to determine a_0^2. In practice, however, this was not possible. Figure 4 compares results obtained for the Goebel-Chew-Low extrapolation function F' in the $(\pi^+\pi^+)$ channel with the corresponding results obtained in the $(\pi^+\pi^-)$ channel. The results shown are for $m^2_{\pi\pi}=4.45$, at 260 and 280 MeV, and are typical of the results at other values of $m_{\pi\pi}$ and T_π. At the incident energies studied in this experiment, the minimum value of $|t|$ attainable experimentally is slightly greater than zero, which explains the sharp drop in F' near $|t|=0$. The same behavior is seen in the phase-space distribution of t. Since the t dependence of F' has no distinguishable linear region in the $(\pi^+\pi^+)$ channel, it was not possible to apply the same formalism to this channel in our energy range. It is interesting to note that the $\cos(\theta)$ distributions measured in the $\pi^+\pi^+$ channel (see Ref. [10]) are not as flat as for the $(\pi^+\pi^-)$ data.

Although mechanisms with Δ intermediate states contribute to the non-OPE background in both channels, charge conservation forbids N^* exchange in the $\pi^+p\to\pi^+\pi^+n$ channel. Therefore it seems rather surprising that the data seem to suggest that OPE dominance can be found in limited kinematic regions of the $\pi^+\pi^-$ channel whereas in the $\pi^+\pi^+$ channel it cannot. We have no rigorous explanation to this puzzle, but offer the following qualitative argument.

The $\pi^+\pi^-$ channel is predominantly isospin zero while only isospin two contributes to the $\pi^+\pi^+$ channel. The threshold cross sections for the two reaction channels can thus be estimated in terms of the S-wave isospin zero and two scattering lengths as $\sigma_{\rm th}^{++}\sim 4\pi(a_0^2)^2$ and $\sigma_{\rm th}^{+-}\sim 4\pi(\frac{2}{3}a_0^0)^2$. Here the small contribution of the isospin two

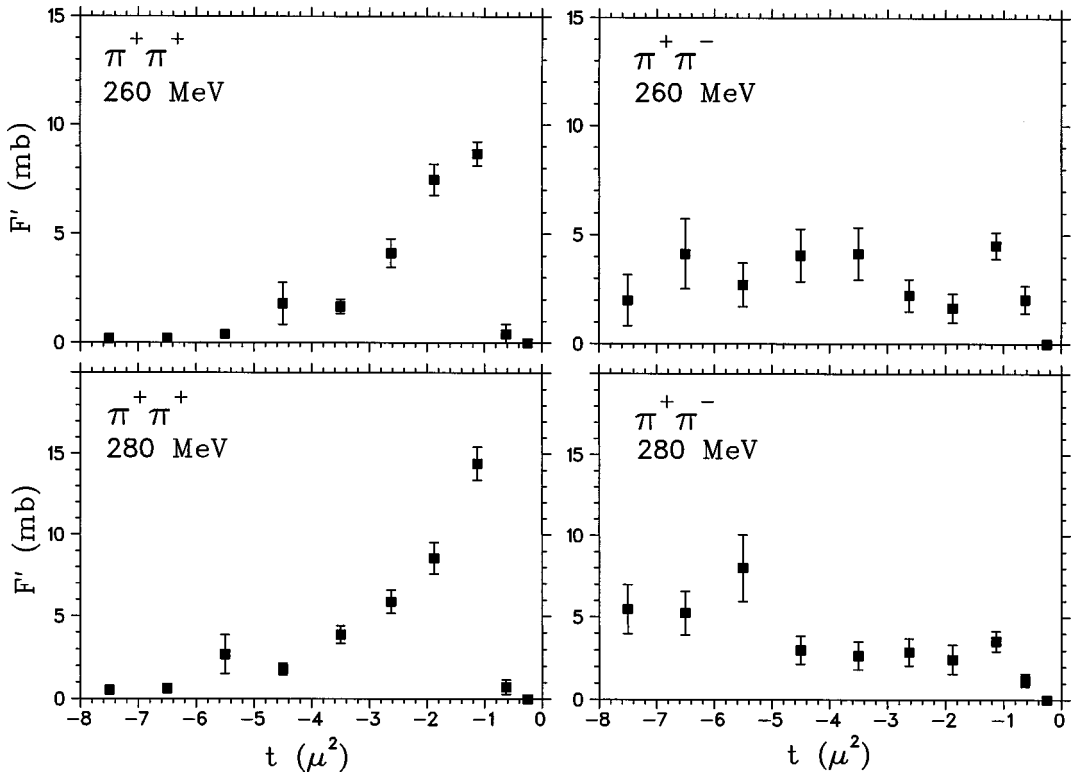

FIG. 4. Typical plots of the Goebel-Chew-Low function, $F'(t,m_{\pi\pi})$, for the $(\pi^+\pi^+)$ channel (left) compared to those obtained in the $(\pi^+\pi^-)$ channel (right) at 280 MeV (upper) and 260 MeV (lower). All results are at $m^2_{\pi\pi}=4.45$. The linearity evident in the $(\pi^+\pi^-)$ results is absent in the $(\pi^+\pi^+)$ results, precluding the application of the Goebel-Chew-Low procedure in the $(\pi^+\pi^+)$ channel.

S-wave scattering length in the $\pi^+\pi^-$ channel has been neglected. Assuming the contribution at threshold is predominantly OPE, and using $a_0^0=0.209\mu^{-1}$ and $a_0^2=-0.041\mu^{-1}$ [13], the ratio of the cross sections is then

$$\frac{\sigma^{+-}_{\rm OPE}}{\sigma^{++}_{\rm OPE}}=\left(\frac{2a_0^0}{3a_0^2}\right)^2\sim 12. \tag{4}$$

On the other hand, at the energies studied in this experiment, the total cross sections for $\pi^-p\to\pi^+\pi^-n$ are about 7 times greater than those for $\pi^+p\to\pi^+\pi^+n$ (see Ref. [10]). In other words,

$$\frac{\sigma^{+-}_{\rm OPE}+\sigma^{+-}_{\rm BKG}}{\sigma^{++}_{\rm OPE}+\sigma^{++}_{\rm BKG}}\sim 7, \tag{5}$$

where $\sigma_{\rm BKG}$ refers to all non-OPE contributions. Combining Eqs. (4) and (5), we obtain

$$\frac{\sigma^{++}_{\rm BKG}}{\sigma^{++}_{\rm OPE}}\sim\frac{12\sigma^{+-}_{\rm BKG}}{7\sigma^{+-}_{\rm OPE}}+\frac{5}{7}. \tag{6}$$

Several interesting observations can be drawn from Eq. (6). First, $\sigma^{++}_{\rm BKG}$ cannot be zero, whereas $\sigma^{+-}_{\rm BKG}$ can be. In fact, $\sigma^{++}_{\rm BKG}/\sigma^{++}_{\rm OPE}$ has to be greater than about 70%, whereas $\sigma^{+-}_{\rm BKG}/\sigma^{+-}_{\rm OPE}$ can be zero. We do not know what value to associate with $\sigma^{+-}_{\rm BKG}/\sigma^{+-}_{\rm OPE}$. However, Eq. (6) implies that whatever it is, the corresponding ratio of background to OPE in the $\pi^+\pi^+$ channel is at least nearly twice as much. For example, if the background is comparable to OPE in the $\pi^+\pi^-$ channel ($\sigma^{+-}_{\rm BKG}/\sigma^{+-}_{\rm OPE}=1$), then the background is 2.4 times larger than OPE in the $\pi^+\pi^+$ channel. It is thus not so surprising after all that the application of the Goebel-Chew-Low formalism to the $\pi^+\pi^+n$ data is problematic, since one is trying to observe a signal which is $\geqslant 2$ times smaller than in the $\pi^-p\to\pi^+\pi^-n$ reaction, relative to the background processes.

V. ROY EQUATIONS

Once the $\pi^+\pi^-$ cross sections were determined, dispersion constraints embodied in the Roy equations were used to check whether the extrapolated cross sections were consistent with results obtained at much higher incident momenta.

Pion-pion phase shifts constrained by unitarity, analyticity, crossing, and Bose symmetry were studied by Roy [33] and Basdevant *et al.* [34,35], resulting in a set of relations known as the ''Roy equations.'' These equations predict partial-wave amplitudes in the threshold and even subthreshold region from $\pi\pi$ amplitudes determined from data in the physical region ($4\leqslant m^2_{\pi\pi}\leqslant 60$). Dispersion-type constraints, expressed in terms of Roy equations, determine $\pi\pi$ amplitudes from high-energy data, which is quite useful given the sparcity of data in the more interesting region below $m_{\pi\pi}\approx 500$ MeV ($m^2_{\pi\pi}\leqslant 13\mu^2$).

One of the most recent attempts to use Roy equations for a model-independent analysis of $\pi\pi$ scattering phase shifts from $\pi N\to\pi\pi N$ was made in Ref. [36]. The average *S*- and *P*-wave phase shifts were determined by fitting all of the then-available experimental data in the dipion mass region up to 1 GeV for 5 reaction channels at large p_π's (within the

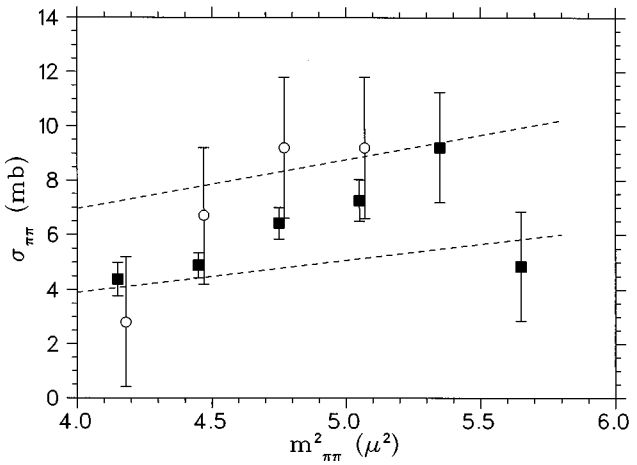

FIG. 5. The cross sections obtained in this experiment (data selection A) plotted against $m^2_{\pi\pi}$. The solid points denote the extrapolated values from the Goebel-Chew-Low analysis, and the open points are from Ref. [8]. The dashed lines represent dispersion constraints from the results of Ref. [36], using the Roy equations, with only higher momenta data included as input.

range 4–15 GeV/c). The Roy equations were then applied to find self-consistent $\pi\pi$-scattering partial amplitudes for the whole $m_{\pi\pi}$ region. The $\pi\pi$ scattering lengths were varied to find the solutions which best described the amplitudes derived from experiment. Partial amplitudes obtained in this way satisfy unitarity, analyticity and crossing constraints in the energy range up to 1 GeV and are completely self-consistent for a restricted range of S-wave scattering lengths $0.205<a_0^0<0.270$, and $-0.048<a_0^2<-0.016$ (in inverse pion mass units). The method is described in detail in Ref. [36].

Given the $\pi\pi$ scattering partial amplitudes, other $\pi\pi$ observables can be calculated for any $m_{\pi\pi}$ from threshold to 1 GeV. The $\pi^+\pi^-$ scattering cross section near threshold is calculated using the following formula:

$$\sigma_{\pi\pi}(\mathrm{mb})=\frac{4\pi}{q^2}(|S|^2+3|P|^2), \tag{7}$$

where

$$S=\frac{2}{3}A_0^0+\frac{1}{3}A_0^2, \quad P=A_1^1, \tag{8}$$

and

$$A_l^I=\sin(\delta_l^I)\times\exp(i\,\delta_l^I) \tag{9}$$

are the partial amplitudes in the elastic region, and $\hbar c=1$. It is interesting to compare the cross sections obtained in the present paper using the Goebel-Chew-Low technique to previously determined values based on the same method [8], as well as those calculated on the basis of phase shifts which were determined in Ref. [36]. As shown in Fig. 5, the present results are consistent with the band of allowed values predicted from the Roy equations using only higher energy data. This fact suggests that the Goebel-Chew-Low method can be applied in the same manner to both high energy and near-threshold $\pi N\to\pi\pi N$ data. The figure also demonstrates that the CHAOS results are in reasonable agreement with the results of Ref. [8]. A determination of a_0^0 using the Roy equations, and including the present $\pi\pi$ cross sections, is discussed in the next section.

VI. SCATTERING LENGTHS

The dipion invariant mass region near threshold is very sensitive to the scattering lengths. In fact, data in the threshold region may be used without any experimental information from higher energies to determine the scattering length. We used the $\pi\pi$ cross sections obtained in this work to determine the S wave, isospin zero $\pi\pi$ scattering length a_0^0 in a variety of ways. Although the methods differ considerably from one another, consistent results for a_0^0 were obtained from each determination.

We begin by collecting a few of the needed expressions. $\sigma_{\pi\pi}$ may be expressed in terms of the S-wave isospin 0 and 2 phase shifts by combining Eqs. (7)–(9), and making use of the approximations $\sin^2\delta_1^1\sim 0$ and $\cos(\delta_0^0-\delta_0^2)\sim 1$. In our $m^2_{\pi\pi}$ range, $\delta_1^1\leqslant 0.2°$, and $\cos(\delta_0^0-\delta_0^2)\geqslant 0.985$ [36]:

$$\sigma_{\pi\pi}\sim\frac{4\pi}{9q^2}(4\sin^2\delta_0^0+\sin^2\delta_0^2+4\sin\delta_0^0\sin\delta_0^2). \tag{10}$$

In our region so close to threshold we can also make use of the threshold approximation:

$$\sin(2\,\delta_l^I)=2\sqrt{\frac{s-4}{s}}[a_l^I+b_l^I\cdot(q/\mu)^2], \tag{11}$$

where $s=m^2_{\pi\pi}$. Combining Eqs. (10) and (11) a useful expression connecting the scattering lengths to $\sigma_{\pi\pi}$ may be obtained:

$$\sigma_{\pi\pi}(s)\sim\frac{16\pi}{9(q/\mu)^2}\left(\frac{s-4}{s}\right)[(a_0^0)^2+a_0^0a_0^2+2a_0^0b_0^0(q/\mu)^2]. \tag{12}$$

Here terms of order q^4 and higher have been dropped, and use has been made of the fact that $\cos\delta_l^I\sim 1$ and $\delta_0^2/\delta_0^0\ll 1$. Using canonical values for a_l^I and b_l^I we find that the terms which have been dropped from Eq. (12) occur in pairs with approximately equal magnitudes [$\sim 1\%$ of the leading $(a_0^0)^2$ term] and opposite signs.

The cross sections $\sigma_{\pi\pi}(s)$ depend only weakly on the value of a_0^2, as one would expect, since the reaction $\pi^-p\to\pi^+\pi^-n$ deals predominantly with the isospin 0 channel. For this reason we can use the well-known correlation

$$2a_0^0-5a_0^2=0.62\pm 0.05 \tag{13}$$

(see, for example, Ref. [38]), which is known as the ''universal curve.''

As a first step we provide an upper limit for a_0^0. The dispersion constraints as well as our results for $\sigma_{\pi\pi}(m^2_{\pi\pi})$ shown in Fig. 5 confirm a trend observed from all other available information, namely, that the slope parameter b_0^0 is positive. Even though the precision with which b_0^0 has been determined in the past has been poor, it is clear that

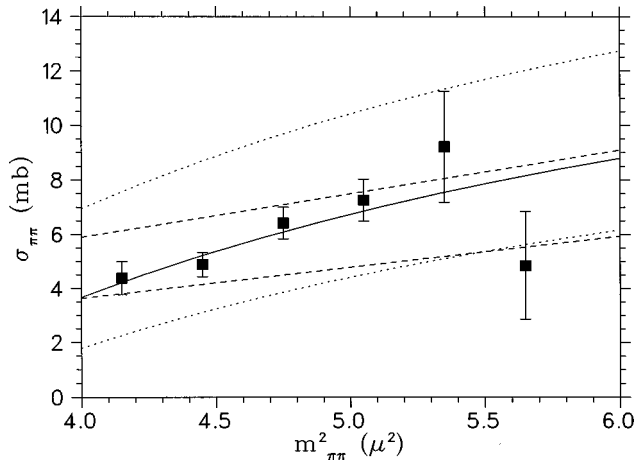

FIG. 6. The cross sections obtained in this experiment plotted against $m^2_{\pi\pi}$. The solid points denote the extrapolated values from the Goebel-Chew-Low analysis (data selection A). The solid line is the result of the threshold expansion fit (Table II), method (1). The dotted lines indicate the results of fixing a_0^0 at 0.26 (upper) and 0.16 (lower), and are provided to highlight the sensitivity to the scattering length in this kinematic regime. The dashed lines represent dispersion constraints from the results of Ref. [36], using the Roy equations, with the present results as well as higher momenta data included as input.

$\sigma_{\pi\pi}(m^2_{\pi\pi})$ is an increasing function of $m^2_{\pi\pi}$. As such the value of the cross section at threshold is not bigger than the average cross section

$$\sigma_{\pi\pi}(4) < \sigma_{av}, \tag{14}$$

where $\sigma_{av} = 5.53 \pm 0.28$ mb is the (weighted) average of the cross sections over our region of $m^2_{\pi\pi}$ (data selection A). Inserting this result into Eq. (12) with $b_0^0 = 0$, and making use of the universal curve to eliminate a_0^2, an analytic solution may be obtained for an upper limit to a_0^0, $a_0^0 \leqslant 0.238 \pm 0.006$.

Next, Eq. (12) is used to determine a_0^0 [method (1)]. The experimental values of $\sigma_{\pi\pi}$ tabulated in Table II were fit using Eq. (12) with a_0^0 and b_0^0 as free parameters, and a_0^2 from the universal curve. The value $a_0^0 = 0.204 \pm 0.014$ was obtained with data selection A. The error quoted here includes the uncertainty in the fit, the statistical error of the data, as well as the ± 0.05 uncertainty ascribed to the universal curve. The fitted slope parameter was $b_0^0 = 0.420 \pm 0.118$. The χ^2_ν of the fit was 1.2. The fit is plotted along with the $\sigma_{\pi\pi}$ in Fig. 6. In order to illustrate the sensitivity to a_0^0 in our region, the fit to Eq. (12) is also plotted in this figure with a_0^0 fixed at two limiting values. The upper dotted curve corresponds to $a_0^0 = 0.26$, which is the K_{e4} result [14]. The lower dotted curve corresponds to the original Weinberg result [37] of $a_0^0 = 0.16$.

In order to estimate the uncertainty in this result associated with the 10% systematic error in the double differential cross sections, the Goebel-Chew-Low analysis and fitting procedure were repeated with the cross sections floated up and down by 10%. The resulting change in a_0^0 was ± 0.008. It would of course also be interesting to estimate the uncertainty associated with the assumption of OPE dominance upon which this work is predicated. Unfortunately, in the absence of any reliable model for the non-OPE background, this was not possible in the present work.

The rest of the methods we now describe may be considered as checks of the first method. A second determination (2) of a_0^0 was made using a one parameter fit, by making use of the approximation [34,14]

$$b_0^0 - a_1^1 = 0.19 - (a_0^0 - 0.15)^2 \pm 0.04, \tag{15}$$

where $a_1^1 = 0.035\mu^{-3}$. In this case, we obtain the result $a_0^0 = 0.229 \pm 0.008$, but the χ^2_ν is 2.1. The reason for the poorer χ^2_ν in this case is that the slope parameter given by Eq. (15) is too flat compared to the data. Equation (15) implies $b_0^0 = 0.184$, whereas in the two parameter fit b_0^0 was determined to be 0.420 ± 0.118.

Method (3) made use of Eq. (10) directly. In this case, the values of δ_0^2 were taken from Ref. [36], and δ_0^0 was determined from fitting the measured $\sigma_{\pi\pi}$values to Eq. (10). The values obtained for δ_0^0 are tabulated in Table II. These phases were then used to determine a_0^0 by fitting the threshold expansion, Eq. (11). In this case we obtain the result $a_0^0 = 0.214 \pm 0.011$.

Methods (1), (2), and (3) were performed for both data selection choices A and B. Table II provides the results of all six combinations.

A fourth determination was made [30] by choosing an even more restrictive data selection (C) than in method B, and performing an energy independent Goebel-Chew-Low analysis [method (4)]. In parallel, using the results of Ref. [36], near-threshold $\pi\pi$ scattering cross sections were calculated as a function of a_0^0 at $m_{\pi\pi}$ values matching those of the present experiment. A χ^2 based on the difference between the experimental (Goebel-Chew-Low) cross sections determined in the energy independent analysis, and those computed using the Roy equations was calculated as a function of a_0^0. We found that χ^2 depended only weakly on the value of a_0^2, as one would expect. However, χ^2 developed a very sharp minimum as a function of a_0^0. Keeping a_0^2 fixed at -0.04, we obtained $a_0^0 = 0.21 \pm 0.02$.

Another way (5) to determine the $\pi\pi$ scattering length is purely within the context of a dispersion analysis, using the Roy equations. The extrapolated $\pi^+\pi^-$ cross sections from this work (Table II), along with appropriate values of δ_0^2 from [36] were used to determine δ_0^0 as a function of $m^2_{\pi\pi}$. These phase shifts were added as input to an analysis performed according to Ref. [36]. The value of a_0^0 obtained was $0.200 < a_0^0 < 0.250$ with a central (optimal) value $a_0^0 = 0.223$. This compares favorably with the previous results of Ref. [36] which quotes a central value of 0.225 and a range $0.205 < a_0^0 < 0.270$.

Our results are also in good agreement with calculations based on chiral perturbation theory to one loop [11] ($a_0^0 = 0.20 \pm 0.01$ and $a_0^2 = -0.042 \pm 0.002$), and more recently to two loops [13] $a_0^0 = 0.217$. In contrast to the standard case, generalized chiral perturbation theory (GChPT) [2] allows for a range of values for the scattering lengths, depending on the value of the quark condensate in the chiral limit. The scattering length obtained from GChPT is $a_0^0 = 0.263$

± 0.052 [2], which corresponds to a small quark condensate. We point out, however, that this value was obtained by fixing one of the parameters in GChPT using the K_{e4} data of Roselet *et al.*, [14]. The Roselet data by themselves lead to a value for a_0^0 of 0.26 ± 0.05. Although the value for a_0^0 found here is more consistent with the Gell-Mann-Oakes-Renner picture, where the quark condensate is large, our result is also within 1σ of the GChPT prediction. Until the accuracy of the GChPT prediction is improved, it will be difficult to discriminate between the two approaches based on any experimental measure of a_0^0. A summary of other *S*-wave scattering length predictions and experimental results may be found, for example, in Ref. [36].

VII. CONCLUSIONS

An exclusive study of the elementary pion induced pion production reactions $\pi^- p \to \pi^+ \pi^- n$ and $\pi^+ p \to \pi^+ \pi^+ p$ at incident pion energies of 223, 243, 264, and 284 MeV was presented. One of the main goals of this experiment was to determine the $\pi\pi$ scattering parameters near threshold. To this end, the experimental $\pi N \to \pi\pi N$ double differential cross sections were used to obtain on-shell pion-pion scattering cross sections via the Goebel-Chew-Low technique.

The Goebel-Chew-Low procedure was applied to the measured $\pi^- p \to \pi^+ \pi^- n$ double differential cross sections over carefully chosen intervals in t, where $F'(t, m_{\pi\pi})$ could be described by a linear function. Stated differently, these were the intervals where the dominance of one-pion-exchange could be assumed. The resulting cross sections are consistent with dispersion constraints based on previously measured $\pi\pi$ observables at higher energies ($m_{\pi\pi} \geqslant 500$ MeV).

Consistent results were obtained using several different methods and data selections to obtain the scattering length a_0^0. Use of the threshold expansion, coupled with the universal curve, provided the result $a_0^0 = 0.204 \pm 0.014$ (statistical) ± 0.008 (systematic) and $b_0^0 = 0.420 \pm 0.118$.

Roy equations were also applied in order to obtain a self-consistent determination of $\pi\pi$ scattering partial amplitudes. Taking into account the present $\pi\pi$ cross sections, the isospin zero *S*-wave scattering length a_0^0 was determined to be $a_0^0 = 0.223^{+0.027}_{-0.023}$.

We have shown that there are significant differences between the reaction mechanisms for the $(\pi^- \pi^+)$ and $(\pi^+ \pi^+)$ channels. An attempt to use the same Goebel-Chew-Low method on the $\pi^+ p \to \pi^+ \pi^+ p$ data failed.

The Goebel-Chew-Low analysis presented in this work was predicated on the assumption of OPE dominance. Arguments supporting this assumption were based primarily on the observation of t intervals linear in F' for a subset of the $\pi^- p \to \pi^+ \pi^- n$ data. However, the linearity of F' does not guarantee the absence of non-OPE signals. This is a valid criticism of this approach and in fact applies to all $\pi N \to \pi\pi N$ data. In the case of the present work, the observation of a *P*-wave contribution in the $\cos(\theta)$ angular distributions ($\leqslant 10\%$ of the *S* wave), coupled with the relatively poor χ^2_ν obtained in the global fits, suggests that some non-OPE background was in fact present. It is, however, reassuring that the results of the current Goebel-Chew-Low analysis are consistent with the phase shifts obtained from the high incident energy data. This work is not meant to prove the validity of the Goebel-Chew-Low technique as a tool for studying $\pi\pi$ scattering. However, it suggests that the Goebel-Chew-Low method can be applied in the same manner to both high energy and threshold $\pi N \to \pi\pi N$ data. In order to circumvent questions associated with the validity of the assumption of OPE dominance, high statistics K_{e4} measurements should ultimately be used to measure a_0^0.

Pion-pion interactions are one of the most fundamental strong interactions, and as such they are of crucial importance to our understanding of the manifestation of QCD in the low-energy domain. However, the experimental study of these processes is not a trivial task, and all experimental $\pi\pi$ scattering data have been obtained via indirect means. Although numerous experiments have been performed to study elementary pion induced pion production reactions (mostly total cross sections and studies in the GeV region), the prescription for determining pion-pion scattering parameters from $\pi N \to \pi\pi N$ data is hampered by theoretical uncertainty and ambiguity. In the recent work of Ref. [12], the chiral expansion of $\pi N \to \pi\pi N$ threshold amplitudes was provided in the framework of heavy baryon chiral perturbation theory. This work improved the theoretical situation near threshold, but the procedure for extracting $\pi\pi$ scattering observables from $\pi N \to \pi\pi N$ data above threshold still remains uncertain. The largest obstacle to extracting $\pi\pi$ scattering observables from $\pi N \to \pi\pi N$ data is the lack of a reliable model for describing the non-OPE background. As a result, the impact of the assumption of OPE dominance made in this work cannot be properly gauged.

Clearly a large theoretical effort is required in order to fully utilize the existing $\pi N \to \pi\pi N$ data to determine accurate pion-pion scattering observables. It is certain that no theoretical effort can be fruitful without significant experimental guidance. The results presented here should play an important role in this arena.

ACKNOWLEDGMENTS

This work was supported by the Natural Sciences and Engineering Research Council (NSERC) of Canada, as well as by the Instituto Nazionale di Fisica Nucleare (INFN), Italy, and the Australian Research Council. One of us (E.F.G.) acknowledges support from the California State University Sacramento (CSUS) Foundation. We also thank the technical and support staff of TRIUMF, especially efforts and talents of the cryogenic target group under the leadership of D. Healey. Some of us (O.P., V.M., V.T.) would like to thank S.T. Belyaev for support. We are pleased to acknowledge discussions and useful remarks from D. Počanic, A.A. Bolokhov, M. Shmatikov, K.N. Muhkin, and V. Vereshchagin.

[1] J. Gasser and H. Leutwyler, Ann. Phys. (N.Y.) **158**, 142 (1984).
[2] M. Knecht, B. Moussallam, J. Stern, and N. H. Fuchs, Nucl. Phys. **B457**, 513 (1995).
[3] J. P. Baton, G. Laurens, and J. Reignier, Nucl. Phys. **B3**, 349 (1967).
[4] C. Goebel, Phys. Rev. Lett. **1**, 337 (1958); G. F. Chew and F. E. Low, Phys. Rev. **113**, 1640 (1959).
[5] B. R. Martin, D. Morgan, and G. Shaw, *Pion-pion Interactions in Particle Physics* (Academic, New York, 1976).
[6] K. N. Mukhin, O. O. Patarakin, Sov. Phys. Usp. **24**, 161 (1981).
[7] W. Ochs, πN Newsletter **3**, 25 (1991).
[8] A. A. Bel'kov, S. A. Bunyatov, B. Z. Zalikhanov, V. S. Kurbatov, A. Khalbaev, V. A. Yarbu, JETP Lett. **29**, 597 (1979).
[9] G. R. Smith *et al.*, Nucl. Instrum. Methods Phys. Res. A **362**, 349 (1995).
[10] M. Kermani *et al.*, Phys. Rev. C **58**, 3419 (1998), preceding paper.
[11] J. Gasser and H. Leutwyler, Phys. Lett. **125B**, 321 (1982); **125B**, 325 (1982).
[12] V. Bernard, N. Kaiser, and Ulf-G. Meißner, Nucl. Phys. **B457**, 147 (1995).
[13] J. Bijnens, G. Colangelo, G. Ecker, J. Gasser, and M. E. Sainio, Phys. Lett. B **374**, 210 (1996).
[14] L. Roselet *et al.*, Phys. Rev. D **15**, 574 (1977).
[15] S. Dubnichka, V. A. Meshcheryakov, and J. Milko, J. Phys. G **7**, 605 (1981).
[16] B. Adeva *et al.*, Report No. CERN SPSLS, 1994.
[17] A. C. Betker *et al.*, Phys. Rev. Lett. **77**, 3510 (1996).
[18] J. A. Jones *et al.*, Nucl. Phys. **B83**, 93 (1974).
[19] G. Kernel *et al.*, Phys. Lett. B **216**, 244 (1988).
[20] G. Kernel *et al.*, Phys. Lett. B **225**, 198 (1989).
[21] G. Kernel *et al.*, Z. Phys. C **48**, 201 (1990).
[22] M. G. Olsson and L. Turner, Phys. Rev. Lett. **20**, 1127 (1968).
[23] M. Sevior *et al.*, Phys. Rev. D **48**, 3987 (1993); Phys. Rev. Lett. **66**, 2569 (1991).
[24] J. B. Lange, *et al.*, Phys. Rev. Lett. **80**, 1597 (1998).
[25] J. Lowe *et al.*, Phys. Rev. C **44**, 956 (1991).
[26] D. Počanic *et al.*, Phys. Rev. Lett. **72**, 1156 (1994).
[27] Emil Frlež, Ph.D. thesis, Los Alamos National Laboratory, Report No. LA-12663-T, 1993.
[28] H. W. Ortner, U. Bohnert, D. Malz, R. Müller, M. Dillig, and O. Jäkel, Phys. Rev. C **47**, R447 (1993).
[29] R. Müller *et al.*, Phys. Rev. C **48**, 981 (1993).
[30] M. Kermani, Ph.D. thesis, University of British Columbia, 1997.
[31] S. B. Treiman and C. N. Yang, Phys. Rev. Lett. **8**, 140 (1962); J. D. Jackson, Nuovo Cimento **34**, 1644 (1964).
[32] P. R. Bevington, *Data Reduction and Error Analysis for the Physical Sciences* (McGraw-Hill, New York, 1977).
[33] S. M. Roy, Phys. Lett. **36B**, 353 (1971).
[34] J. L. Basdevant, C. D. Frogatt, and J. L. Petersen, Nucl. Phys. **B72**, 413 (1974).
[35] J. L. Basdevant, J. C. Le Guillou, and H. Navelet, Nuovo Cimento A **7**, 363 (1972).
[36] O. O. Patarakin, V. N. Tikhonov, and K. N. Mukhin, Nucl. Phys. **A598**, 335 (1996).
[37] S. Weinberg, Phys. Rev. Lett. **17**, 616 (1966); **18**, 188 (1967).
[38] O. Dumbrais, R. Koch, H. Pilkuhn, G. C. Oades, H. Behrens, J. J. deSwart, and P. Kroll, Nucl. Phys. **B216**, 277 (1983).